Diamond & Related Materials 91 (2019) 119–126

Contents lists available at ScienceDirect

Diamond & Related Materials

journal homepage: www.elsevier.com/locate/diamond

Xanthoceras sorbifolia seed coats derived porous carbon with unique architecture for high rate performance supercapacitors

Yan-Lei Zhang*, Shi-Ying Li, Zhi-Shu Tang, Zhong-xing Song, Jing Sun

Shaanxi Collaborative Innovation Center of Industrialization of Traditional Chinese Medicine Resources, Shaanxi University of Chinese Medicine, Xianyang 712083, PR China

ARTICLE INFO

Keywords:
Biomass derived
Biomaterials
Carbon materials
Porous materials
Electrochemical properties

ABSTRACT

Here in this report, *Xanthoceras sorbifolia* seed coats are selected to prepare porous carbons. Biochar is first prepared by dry distillation of the seed coats, and then is transformed into porous carbon by KOH activation. The regulation of activation temperatures and ratios of activator is studied. The optimized condition is activation temperature of 750 °C, and the ratio of biochar to activator is 1:3. HRTEM, X-ray diffraction and the Brunauer-Emmett-Teller methods were used to characterize the samples. The porous carbon prepared under the optimum condition has a specific surface area of 2148 $m^2 g^{-1}$ with a large amount of micropores of about 0.5 nm–2 nm closely and orderly distributed, together with a certain number of mesporous (~12% of the total specific surface area), such a unique structure provides both a large storage space for electrons and a channel for them to passage quickly. Due to this unique architecture, the specific capacitance of the porous carbon is as high as 421 F/g at a current density of 0.5 A/g, with a moderate rate capability (259 F/g at 10 A/g), and good cycle stability (90.7% capacitance retention after 5000 cycles at 10 A/g), suggesting it one of the ideal materials for the development of supercapacitors. Symmetrical supercapacitor based on this material has also been assembled and tested to further verify the actual capacitance properties. The specific capacitance of the symmetrical supercapacitor is 276 F/g at 0.5 A/g, and 50 F/g was achieved when the current density was raised up to 10 A/g. Under the current density of 10 A/g, the capacitance only decreased slightly after the circulation of 5000 cycles, and the retention rate reached 86%, illustrates the practical application potential of this material.

1. Introduction

Xanthoceras sorbifolia is a kind of woody oil plant, mainly distributed in northern region of China. The oil content of its seed kernel is up to 65%, it is a high-quality edible oil contains a valuable ingredient called neuroacid, which is good for human brain [1]. Besides, the oil contains a large amount of Free Fat Acids while with low acid value, makes it an ideal resource for biodiesel production [2,3]. The tree also with great adaptability to arid and cold environments makes it one of the ideal tree species for windbreak and sand fixation in these areas. Therefore, the Chinese government strongly supports the promotion of this tree species, it is estimated to planted up to 5×10^5 ha by 2020 [4]. During the process of harvesting kernels for oil extraction, a large amount of husks and seed coats are produced. There have been many studies on husks, which were used to develop medicines, biofuel, biochar and other high value-added products [1]. But the seed coat, which accounts for more than 50% of the seed's biological mass, has been neglected. The seed coat is rich in lignin, cellulose and other raw materials. It is an ideal resource for the preparation of xylose, wood tar, wood vinegar and activated carbon. However, other than one report that it could be used to remove cationic dyes from water [5], so far, it has not been well developed or utilized. It is normally treated as waste in harvesting kernel for oil extraction, resulting in waste of resources. Therefore it is urgent for us to develop high value-added utilization of this resource.

Ever since they were invented, supercapacitors have never failed to attract our attentions [6]. Compared with batteries, supercapacitors have a faster transmission of power, and a higher rate of recharging [7]. The core problem of supercapacitor research is electrode materials [8]. These materials include metal oxides, porous carbon materials and so on. Among these materials, porous carbon material is a hot spot, because of its high specific surface area and excellent capacitance. A variety of original materials, including biomass and non-biomass-derived [9], are used to prepare porous carbons for supercapacitors and other utilization. These carbon materials come in various forms, such as carbon nanotubes [10], graphene [11], and the preparation process

* Corresponding author.
E-mail address: nwuzyl@163.com (Y.-L. Zhang).

https://doi.org/10.1016/j.diamond.2018.11.013
Received 10 October 2018; Received in revised form 10 November 2018; Accepted 15 November 2018
Available online 16 November 2018
0925-9635/

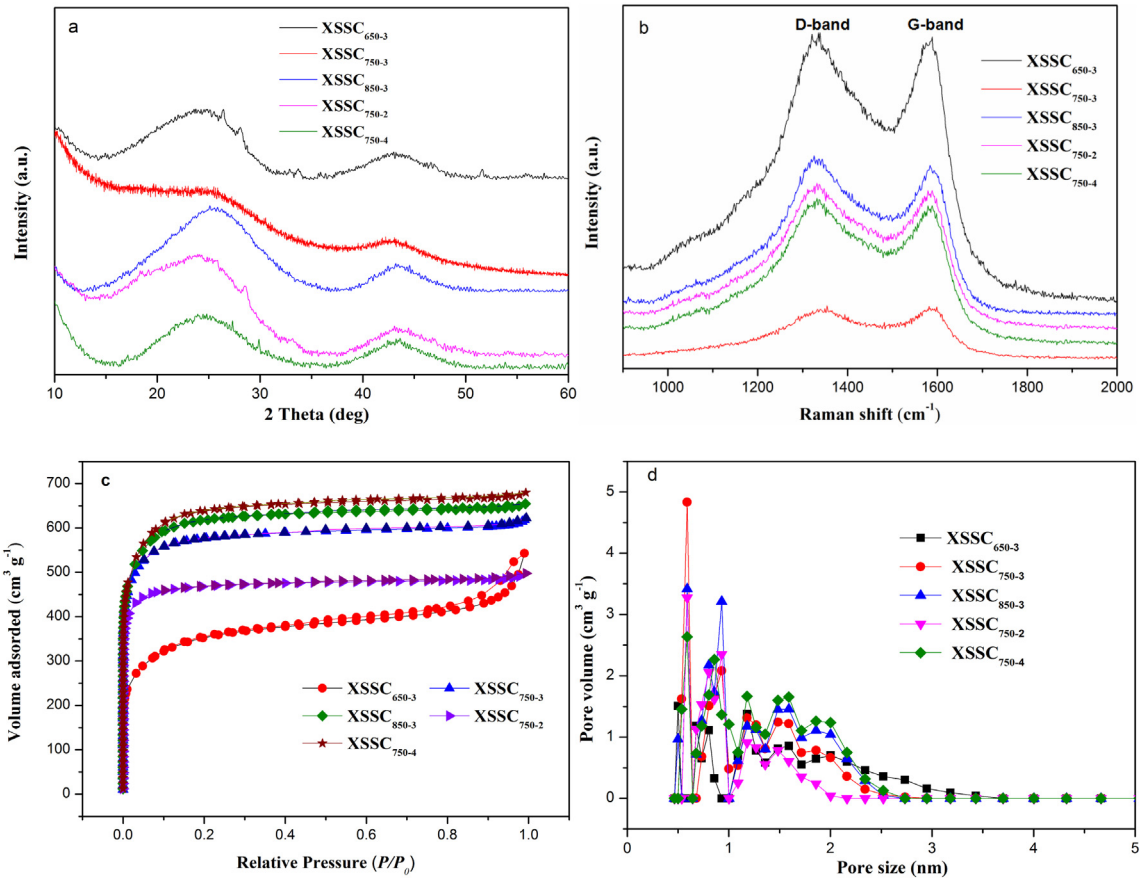

Fig. 1. (a) XRD patters of $XSSC_{a\text{-}b}$, (b) Raman spectra, (c) N_2 adsorption-desorption isotherms, (d) pore-size distributions.

Table 1
Pore structures of the samples and the specific capacitances of samples under 0.5 A/g.

Samples	S_{BET} ($m^2 g^{-1}$)	S_{mic} ($cm^2 g^{-1}$)	S_{mes} ($cm^2 g^{-1}$)	V_{total} ($cm^3 g^{-1}$)	SC (F/g)
$XSSC_{650\text{-}3}$	1284	660	624	0.84	356
$XSSC_{750\text{-}2}$	1814	1621	193	0.77	212
$XSSC_{750\text{-}3}$	2148	1910	238	0.96	423
$XSSC_{750\text{-}4}$	2445	1893	552	1.05	248
$XSSC_{850\text{-}3}$	2337	1840	497	1.01	150

varies. Coal [12,13], petroleum coke [14], coal tar [15], and other non-biological carbon materials are ideal raw materials for the preparation of these kinds of porous carbons [16]. However, the capacitance values of these non-biomass derived materials are usually relatively low, and it is usually necessary to improve the performance by sacrificing templates [17], and doping elements such as nitrogen [18], sulfur [19], and even metal and metal oxides [20], therefore, the preparation cost and the complexity of the process are increased. In contrast, porous carbon materials derived from biomass as cornstalk [21], egg [22], pollen [23], cashmere [24], bamboo [25], tree leaves [26], shrimp shell [27], human hair [28], are usually with better performances and easier preparation processes. Rationally designed porous carbons derived from biomass usually with unique architectures as 3D hierarchical [29,30], which can also be used for CO_2 capture [31,32]. This may be attributed to the fact that the biomass or biomass derived materials usually with unique architectures themselves that are retained during the activation process, and they may also contain certain amount of heteroatoms such as nitrogen, calcium and so on, since the existence of heteroatoms is considered to be one of the important factors to improve the capacitances [33,34], and the presence of elements such as calcium avoids the use of extra templates [35].

The preparation of porous carbon from biomass is generally by first pyrolysis or hydrothermal of the biomass to biochar [36,37], and then different activators, such as KOH, $ZnCl_2$ [38], etc. are used for activation. The process of preparing porous carbon by one-step activation of biomass with potassium ferrate has also been reported [39]. However, KOH activation is by far the most widely used and effective method [40,41]. During the process of prepare biochar by pyrolysis and hydrothermal, usually only biochar is obtained, while by dry distillation, wood vinegar can be obtained simultaneously, which is also an important chemical raw material, widely used in agriculture and other fields [42]. In addition, activated carbon produced by dry distillation also produces unique pore structures [43].

In view of the excellent performance of porous carbons derived from biomass in supercapacitors and other areas, and also considering the abundance of the *Xanthoceras sorbifolia* seed coats (XSBC). Here in this paper, we will provide a method of preparing porous carbon by using XSBC as the raw material, and its application in the fabrication of supercapacitors. This study will provide a new raw material for supercapacitors and also a new way for the waste utilization of XSBC.

2. Experimental

After the kernels were isolated for oil extraction, the seed coat was dried and placed in a dry distillation unit with a condensation system, and heated to 300 °C from room temperature at a heating rate of 3 °C min^{-1}. It was maintained at the final temperature for 3 h, then cooled naturally to room temperature to prepare *Xanthoceras sorbifolia* seed coat biochar (XSSCB). The prepared biochar and KOH were then mixed in different proportions and placed in a quartz boat and transferred to a tube furnace in a nitrogen atmosphere of 200 mL min^{-1},

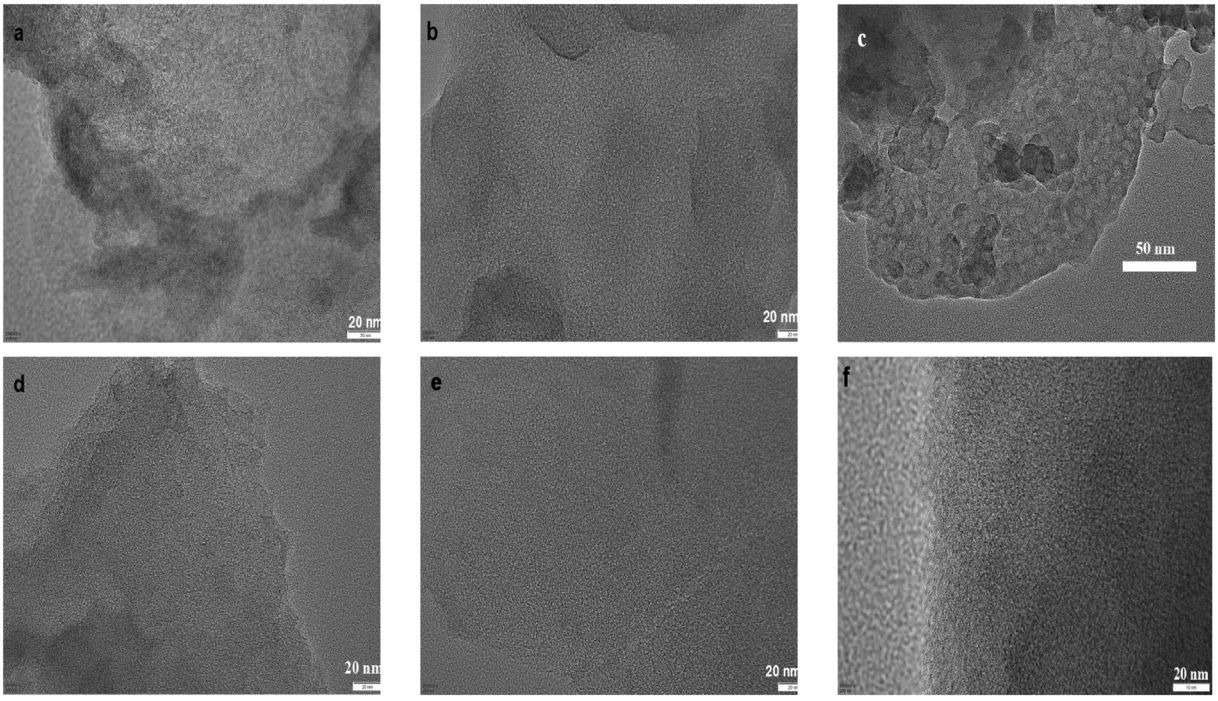

Fig. 2. HRTEM images of (a) $XSSC_{650\text{-}3}$, (b) $XSSC_{750\text{-}2}$, (c and f) $XSSC_{750\text{-}3}$, (d) $XSSC_{750\text{-}4}$, (e) $XSSC_{850\text{-}3}$.

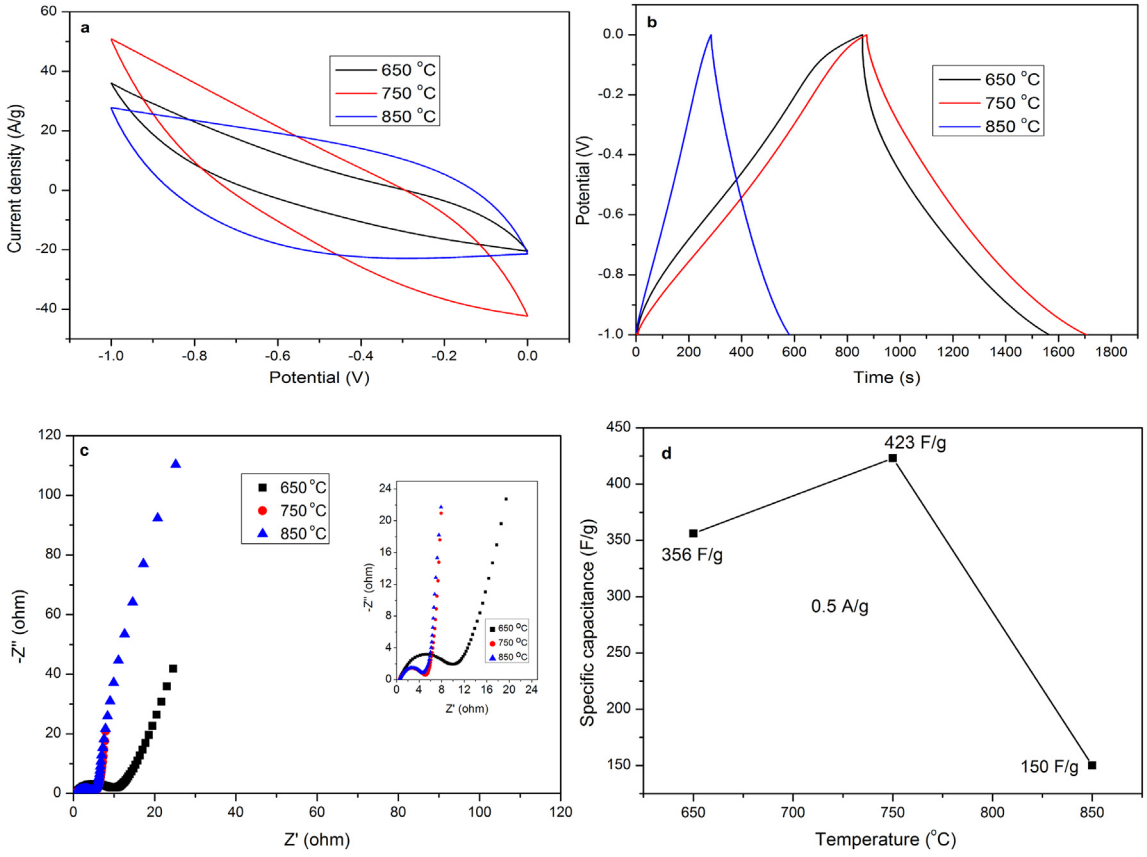

Fig. 3. (a) The CV curves of samples at a scant rate of 200 mV s^{-1}. (b) The galvanostatic charge-discharge curves of samples at a current density of 0.5 A g^{-1}. (c) Nyquist plot of impedance from 0.01 Hz to 100 kHz. (d) Specific capacitance as a function of current density.

heated to different temperatures at a heating rate of 5 °C min^{-1} and maintained at the final temperature for 2 h. The products were washed repeatedly with dilute HCl and distilled water until the filter was near neutral, dried overnight at 80 °C. To investigate the effect of activation temperature and dosage of activator on the performance of porous carbons, different activation temperatures (650, 750, 850 °C) and activator dosage (1:2, 1:3 and 1:4 of biochar to KOH) were used respectively. The final products are marked as $XSSC_{a\text{-}b}$, where a and b

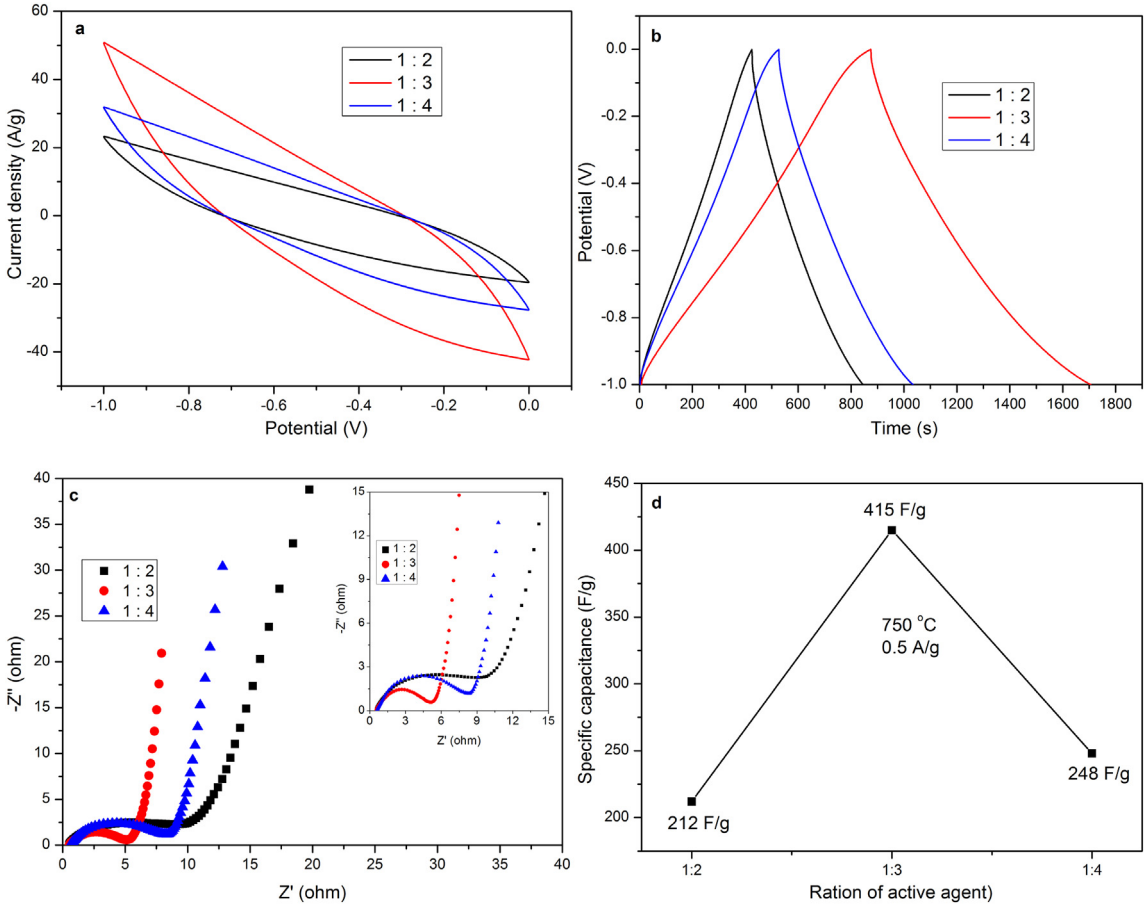

Fig. 4. Electrochemical performances of samples prepared with variation of activator dosage. (a) The CV curves of samples at a scant rate of 200 mV s^{-1}. (b) The galvanostatic charge-discharge curves of samples at a current density of 0.5 A g^{-1}. (c) Nyquist plot of impedance from 0.01 Hz to 100 kHz. (d) Specific capacitance as a function of current density.

represent the activation temperature and the ratio of KOH to biochar. The microstructures and morphology of the samples were characterized by high resolution transmission electron microscopy (HRTEM, JEOL 2100F), X-ray diffraction (XRD, Philips X, pert Prosuper, Cukα, Radiation), and pore structure measurement was processed using nitrogen isothermal adsorption method (ASAP 2020).

To fabricate the test electrodes, samples prepared from *Xanthoceras sorbifolia* seed coat, acetylene black as conductive additive and polytetrafluoroethylene (1%) as binders were fully ground and mixed at a ratio of 8:1:1 and grind thoroughly in an agate mortar. For the three-electrode system, the mixture was evenly coated on a nickel foam (1.5 cm long and 1 cm in width) by a doctor's blade in 1 cm × 1 cm area, and the electrodes were then dried at 120 °C in a vacuum overnight. The dried electrode sheets were weighed after being compressed (~0.3 mm in thickness), the mass loading of the active materials on each electrode was about ~3 mg. Electrochemical properties were tested on a CHI-660 E electrochemical workstation at room temperature, using a Pt sheet as counter electrode and Ag/AgCl as reference electrode in 6 M KOH aqueous. Cyclic voltammetry (CV) curves were measured in a potential range of −1.0–0 V vs Ag/AgCl by varying the scan rate from 0.005–0.2 V/s. Galvanostatic charge/discharge (GC) measurements were processed under a constant current density of 0.5–20 A/g, with a potential window of −1.0–0 V. The cycling stability was tested using the GC measurement at the current density of 10 A/g for 5000 cycles. Electrochemical impedance spectroscopy (EIS) measurements were processed in a frequency range of 100 kHz to 0.01 Hz. Nyquist plots were used to analyze the EIS data.

For the three-electrode system, the specific capacitance (C, F/g) of the samples were calculated from GC curves using the following equation:

$$C = I\,\Delta t/(m\,\Delta V) \quad (1)$$

where I is the current; Δt is the discharge time; m (mg) is the mass loading of the active matters; and ΔV is the voltage change after the IR drop.

For the two-electrode system, the sample mixture was evenly coated on a piece of round nickel foam (1.0 cm in diameter) and pressed (0.3 mm in thickness, mass of the active materials was ~4 mg) after dried, a CR2032 stainless coin type cell was then assembled symmetrically in a glove box filled with argon using the dried electrodes as working electrodes and glass paper as the separator. Cyclic voltammetry (CV) curves were measured in a potential range of 0–1 V by varying the scan rate from 0.005–0.2 V/s. Galvanostatic charge/discharge (GC) measurements were processed under a constant current density of 0.5–5 A/g, with a potential window of 0–1.0 V. The cycling stability was tested using the GC measurement at the current density of 10 A/g for 5000 cycles. Electrochemical impedance spectroscopy (EIS) measurements were also processed in a frequency range of 100 kHz to 0.01 Hz. Nyquist plots were used to analyzed the EIS data.

For the two-electrode system, the specific capacitance (C, F/g) of the samples was calculated from GC curves using the following equation:

$$C = 2I\,\Delta t/(m\,\Delta V) \quad (2)$$

where I is the current; Δt is the discharge time; m (mg) is the mass loading of the active matters on a single electrode; and ΔV is the voltage change after the IR drop.

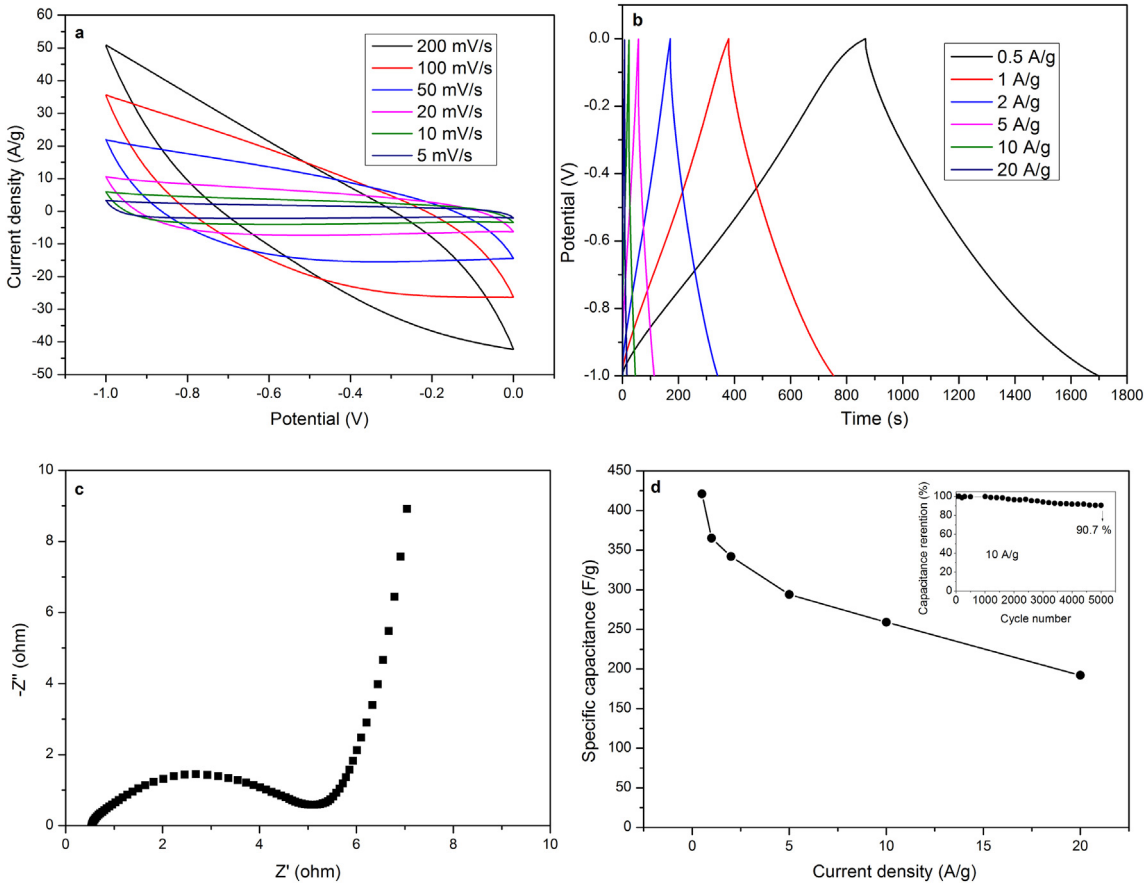

Fig. 5. Electrochemical performances of $XSSC_{750\text{-}3}$: (a) CV curves at different scan rates from 5 to 200 mV s^{-1}; (b) charge-dischagre curves at different current densities from 0.5 to 20 A/g; (c) Nyquist plot of impedance from 0.01 Hz to 100 kHz; (d) specific capacitance as a function of current density, and cycling performance for 5000 cycles loaded at a current density of 10 A/g.

3. Results and discussion

Fig. 1(a) shows the XRD patterns of the samples. The samples showed two wide peaks at 23.6° and 43.7°, indicating their graphitic structures [44]. Raman spectrum of the samples is shown in Fig. 1(b), two distinct peaks at ~1340 cm^{-1} and ~1590 cm^{-1} are detected, representing the D and G bands of disordered carbon and graphite carbon respectively, which matches the XRD patters. The results obtained above infer that these samples possess a certain degree of graphitization while having disordered and amorphous structures [45].

Fig. 1(c) and (d) show the results of nitrogen adsorption-desorption isotherms and the pore size distributions of the samples. According to the classification of IUPAC, the samples $XSSC_{750\text{-}2}$, $XSSC_{750\text{-}3}$, $XSSC_{750\text{-}4}$, and $XSSC_{850\text{-}3}$ display typical type-I isotherms and the sample $XSSC_{650\text{-}3}$ exhibits type-IV isotherm. When the low relative pressures (p/p_0) are below 0.1, the amount of nitrogen adsorbed by all the samples increased sharply, indicating the existence of a large amount of micropores [46]. The small increase of nitrogen adsorption amount after the relative pressure exceeded 0.1 is caused by mesoporous. For the sample $XSSC_{650\text{-}3}$, in the range of relative pressures from 0.45 to 0.98, the hysteresis loop is also obvious, which exhibits typical type-IV adsorption isotherm, further indicating the existence of certain number of mesoporous in this sample. Based on the above results, it is speculated that these samples are mainly composed of micropores with a small number of mesoporous, especially for the $XSSC_{650\text{-}3}$, which has a large number of mesoporous. These results are in perfect agreement with the pore size distributions of the samples shown in Fig. 1(d). The specific surface area, pore volume and pore size distributions of the samples are summarized in Table 1. By comparing the samples prepared under different conditions, it can be seen that the increase of activation temperature and the proportion of activator can help to increase the specific surface area of the samples, and the decrease of activation temperature or the increase of the proportion of activator can increase the amount of mesoporous.

Fig. 2 shows the HRTEM images of the samples, it can be observed clearly that all samples with a large amount of irregular micropores and certain number of mesoporous, except for the sample $XSSC_{750\text{-}3}$ with micropores consistent in size and regularly arranged (Fig. 2c), which can further be seen in Fig. 2f.

After the material preparation and structure characterization, the supercapacitance properties of the materials prepared under different activation conditions were tested and evaluated. We first investigated the effect of activation temperatures on the performance of porous carbons using a three-electrode system. Fig. 3a shows the CV curves of the samples prepared under different temperatures varied from 650 °C to 850 °C with the activator dosage of 1:3 (biochar to KOH). At a scan rate of 200 mV s^{-1}, the CV curves all possess relatively regular and symmetrical spindle shapes, with no obvious redox peaks, inferred them typical EDLC supercapacitors [47]. The loop area of sample $XSSC_{750\text{-}3}$ is larger than those of the other two samples, indicating a higher specific capacitance [48]. This is consistent with the GCD results shown in Fig. 3b, at a current density of 0.5 A/g, the specific capacitance of the sample $XSSC_{750\text{-}3}$ is the highest among them, reaching up to 423 F/g. This is a very high value of specific capacitance compared with other porous carbons derived from biomass or non-biomass reported in literatures.

Fig. 3d is the Nyquist plot of the three samples in a frequency range of 100 kHz to 0.01 Hz. Nyquist plot reflects the electrochemical

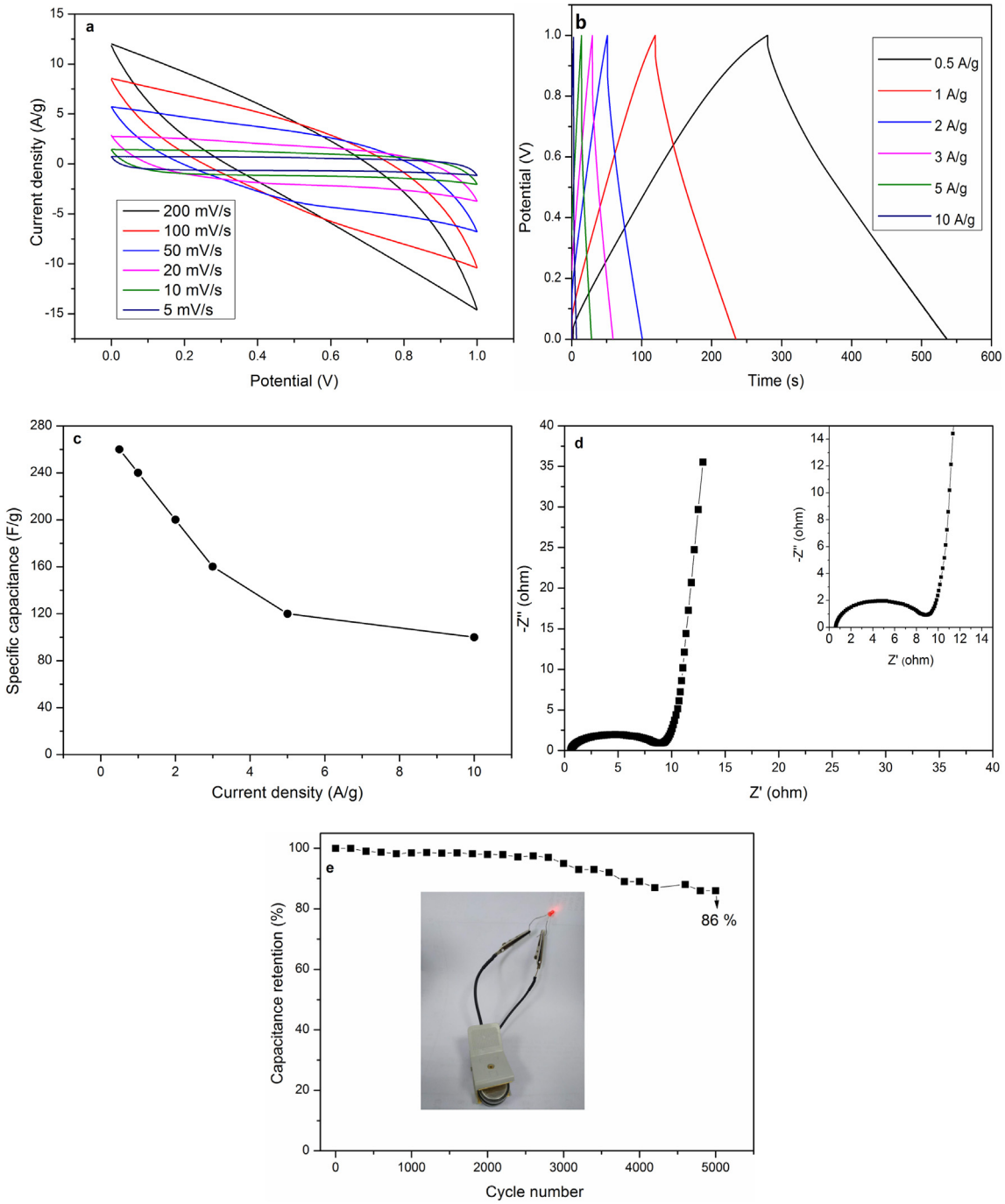

Fig. 6. Electrochemical performances of symmetric supercapacitor fabricated by $XSSC_{750\text{-}3}$: (a) CV curves at different scan rates from 5 to 200 mV s^{-1}; (b) charge-discharge curves at different current densities from 0.5 to 20 A/g; (c) Nyquist plot of impedance from 0.01 Hz to 100 kHz; (d) specific capacitance as a function of current density; (e) cycling performance for 5000 cycles loaded at a current density of 10 A/g, and the assembled supercapacitor lights a LED bead (insert).

impedance spectroscopy (EIS) of the electrode materials. The Nyquist diagram consists of three parts. In the high frequency, the value of the intersection with the Z′ axis represents the overall resistance, also known as the series resistance and the solution resistance (R_S). This part of resistance comes from electrode materials, electrolyte and the current collector and so on. The interfacial charge transfer resistance (R_{ct}) is related to the diameter of the arc in the middle frequency region. Finally, the Warburg impedance related to the slop of the inclined straight line that is in the middle frequency, this part of resistance comes from the diffusion of the ions in the electrolyte. The Nyquist plot of the $XSSC_{750\text{-}3}$ in Fig. 3d is nearly vertical in the low-frequency region, the intercept with the Z′ axis is near the 0 point, and the diameter of the arc in the high-frequency region is about 4 Ω, indicating that the material has a smaller mass transfer resistance compared with the other two samples [49]. Thus, 750 °C was selected as the optimal activation temperature.

With the optimal activation temperature in hand, we next investigated the effect of activator dosage on the supercapacitance values of the samples. At the activation temperature of 750 °C, the activator ratios of 1:2, 1:3 and 1:4 (biochar to KOH) were used respectively, and the specific capacitances of the activated products $XSSC_{750\text{-}2}$, $XSSC_{750\text{-}3}$, and $XSSC_{750\text{-}4}$ were tested. Fig. 4(a) is the CV curves of the samples at a scan rate of 200 mV s^{-1}, GCD results are shown in Fig. 4(b), and Fig. 4(c) is the Nyquist plot of the three samples in a frequency range of

Table 2
Comparison of specific capacitances of the reported works.

Precursors	Preparation of biochar	BET ($m^2 g^{-1}$)	Test system[a]	Electrolyte	Specific capacitance (F/g)	Ref
Lotus pollen	Hydrotherm	3037	2 E	1 M $TEABF_4$/AN	210 (1 A/g)	23
Cashmere	Pyrolysis	1358	2 E	1 M $TEABF_4$/PC	31 (1 A/g)	24
Bamboo	Pyrolysis	1732	3E	6 M KOH	222 (0.5 A/g)	25
Tree leaves	Hydrotherm	1868	3 E	6 M KOH	367 (0.5 A/g)	26
Shrimp shell	Pyrolysis	1113	3 E	6 M KOH	350 (0.5 A/g)	27
Human hair	Pyrolysis	1306	3 E	6 M KOH	340 (1 A/g)	28
Paulownia flower	Pyrolysis	224.8	3 E	1 M H_2SO_4	297 (1 A/g)	49
Seaweeds	Hydrotherm	746	3 E	1 M H_2SO_4	264 (0.2 A/g)	51
Protein	Pyrolysis	805	3 E	1 M H_2SO_4	390 (0.2 A/g)	52
XSSC	Dry distillation	2148	3 E	6 M KOH	421 (0.5 A/g)	This work

[a] 2E/3E refers to a two/three-electrode system.

100 kHz to 0.01 Hz. It can be deduced from both the CV and GCD curves that the sample $XSSC_{750\text{-}3}$ possesses the highest capacitance of 415 F/g among them, while for the samples $XSSC_{750\text{-}2}$ and $XSSC_{750\text{-}4}$, capacitances are 212 F/g and 248 F/g respectively, as shown in Fig. 4(d). From Fig. 4(c) we can see that the Nyquist plot of the $XSSC_{750\text{-}3}$ is more vertical in the low-frequency region, the intercept with the Z′ axis closer to zero point, and the interfacial charge transfer resistance is less than 5 Ω, smaller than those of the other two samples, indicating a smaller mass transfer resistance. It is worth mentioning that although samples $XSSC_{850\text{-}3}$ and $XSSC_{750\text{-}4}$ have larger specific surface areas of 2337 $m^2 g^{-1}$ and 2445 $m^2 g^{-1}$, their specific capacitances are only 150 F/g and 248 F/g respectively, compared with porous carbons derived from other biomass or non-biomass, these are moderate capacitance values, which also indicates that the XSSC has great potential in the preparation of energy-storing porous carbon materials. However, they are much lower than that of the sample $XSSC_{750\text{-}3}$ (The pore structures and specific capacitances of samples at 0.5 A/g are listed in Table 1). This result may be attributed to the fact that the sample $XSSC_{750\text{-}3}$ possesses more microporous with a certain number of mesoporous, and the pores are regularly and tightly distributed, this provides a large specific surface area for storage of electrodes, and the existence of mesoporous is more conducive to rapid and orderly passage of electrons, thus, it exhibits excellent specific capacitance performance. Therefore, the final optimized condition is activation temperature of 750 °C, and the ratio of biochar to activator is 1:3.

Electrochemical performances of $XSSC_{750\text{-}3}$ were then tested and the results obtained after repeated for three times are shown in Fig. 5. At different scan rates from 0.2 V/s to 0.005 V/s, the CV curves all exhibit smooth, regular near symmetric spindle shapes without obvious redox peaks, which conforms to a typical double-layer capacitor structure (Fig. 5a). At a current density of 0.5 A/g, the specific capacitance is 421 F/g, when the current density is raised up to 10 A/g, the specific capacitance can still be 259 F/g with a retention of 61.52% (Fig. 5b), exhibits a moderate rate capability. After 5000 cycles under the current density of 10 A/g, the specific capacitance retention is as high as 90.7% (Fig. 5d, insert), shows high cycle stability. The Nyquist plot of the $XSSC_{750\text{-}3}$ is nearly vertical in the low-frequency region, the intercept with the Z′ axis is closer to the zero point about 0.5 Ω, and the diameter of the arc in the high-frequency region is smaller, indicating that the sample $XSSC_{750\text{-}3}$ has a smaller mass transfer resistance (Fig. 5c).

To further text the actual capacitance of the $XSSC_{750\text{-}3}$, a two-electrode coin type symmetric supercapacitor was fabricated and the electrochemical performances are shown Fig. 6. The results are similar to those in the three-electrode system, the symmetrical spindle CV curves were obtained at different scan rates from 5 to 200 mV s^{-1}, indicating that the sample $XSSC_{750\text{-}3}$ with good rate performance (Fig. 6a). The GC curves show nearly symmetrical triangles in the range of current densities of 0.5–10 A/g, which indicates that it has good reversible charge-discharge performance (Fig. 6b). The specific capacitances were calculated from the GC curves at different current densities from 0.5–10 A/g, the results are shown in Fig. 6c. A high specific capacitance of 276 F/g was obtained at 0.5 A/g, which is much higher than those of the reported biomass-derived porous carbons in 6 mol/L electrolyte [50,51] (The comparison results of specific capacitance properties of porous carbon materials derived from different biomass are shown in Table 2). Surprisingly, when the current density was increased 20 folds to 10 A/g, a capacity retention of 38% was achieved. Fig. 6d shows the Nyquist plot of the symmetric supercapacitor based on the $XSSC_{750\text{-}3}$, in the frequency region ranging from 0.01 to 100 kHZ. At a low frequency region, the vertical lines indicate that the symmetric supercapacitor with the property of EDLC, together with good specific capacitance and high cycle stability. The insert is the Nyquist plot in the high frequency region, the 45° segment (Warburg-type lines) with a short length indicates that the ion transportation resistance is low and ion diffusion efficiency is high. The obtained equivalent series resistances obtained was about 0.5 Ω, confirmed good conductivity of $XSSC_{750\text{-}3}$. Fig. 6e is the specific capacitance retention of the $XSSC_{750\text{-}3}$ based symmetrical supercapacitor at a current density of 10 A/g with 5000 cycles. After 5000 cycles, 86% of the initial capacitance was achieved with slightly decrease, which well matches the results of the Nyquist plot. Furthermore we also assembled a coin type supercapacitor device based on $XSSC_{750\text{-}3}$ to light a LED bead, and it worked smoothly (insert of Fig. 6), which directly further exhibited the excellent performance of this material in supercapacitor.

4. Conclusions

Xanthoceras sorbifolia seed coats have been turned in to porous carbons by a two-step process. Biochar was first prepared by dry distillation of the seed coats and then was activated by KOH. Porous carbon with unique structure is obtained by regulating the dosage of activator and activation temperatures. The optimized condition is activation temperature of 750 °C, and the ratio of biochar to activator is 1:3. The porous carbon prepared under this condition has a specific surface area of 2148 $m^2 g^{-1}$ with a large amount of micropores closely and orderly distributed, together with a certain number of mesoporous (~12% of the total specific surface area), such a unique structure provides both a large storage space for electrons and a channel for them to passage quickly. It is just contributed to this unique structure, that the high specific capacitance of this material is high up to 421 F/g at a current density of 0.5 A/g, and a capacitance of 259 F/g was achieved when the current density enhanced to 10 A/g with a moderate rate capability. Good cycle stability was also obtained with 98.7% capacitance retention after 5000 cycles at 10 A/g. Suggesting it one of the ideal materials for the development of supercapacitors. Symmetrical supercapacitor based on this material has also been assembled and tested to further verify the actual capacitance properties of the material. The specific capacitance of the symmetrical supercapacitor is 276 F/g at 0.5 A/g, and 100 F/g when the current density is raised up to 10 A/g. Under the current density of 10 A/g, the capacitance only decreased slightly after the circulation of 5000 cycles, and the retention rate reached 86%, illustrates the practical application potential of the

material. This study will provide a new raw material for supercapacitors and also will pave a new way for the utilization of XSBC.

Acknowledgments

We thank the finical support from Shaanxi Provincial Key Industries Innovation Chain Project (2018ZDCXL-SF-01-06) and the Shaanxi Provincial Innovation Talent Promotion Program-Science and Technology Innovation Team Project (2018 TD-005). The authors also thank Zhang Nan from Shen Zhen senior High School and Zhang Na from Shaanxi Yan'an Middle School for their assistance in the process of completing the paper.

References

[1] Z.Y. Yao, J.H. Qi, L.M. Yin, Biodiesel production from *Xanthoceras sorbifolia* in China: opportunities and challenges, Renew. Sust. Energ. Rev. 24 (2013) 57–65.
[2] Y.N. Hao, X.M. Wang, L.J. Ding, Preparation of bodiesel from *Xanthoceras sorbiflia* Bunge seed oil, Adv. Mater. Res. 183–185 (2011) 1777–1782.
[3] Y.J. Fu, Y.G. Zu, L.L. Wang, N.J. Zhang, W. Liu, S.M. Li, S. Zhang, Determination of fatty acid methyl esters in biodiesel produced from yellow horn oil by LC, Chromatographia 67 (2008) 9–14.
[4] X.Z. Zhou, X.F. Lu, Z.F. Zhang, H.J. Liu, Z.Q. Lei, *Xanthoceras sorbifolia* husks-derived porous carbon for sodium-ion and lithium-sulfur batteries, Diam. Relat. Mater. 85 (2018) 104–111.
[5] Z. Yao, L. Wang, J. Qi, Biosorption of methylene blue from aqueous solution using a bioenergy forest waste: *Xanthoceras sorbifolia* seed coat, Clean 37 (2009) 642–648.
[6] P. Simon, Y. Gogotsi, B. Dunn, Where do batteries end and supercapacitors begin? Science 343 (2014) 1210–1211.
[7] Y. Shu, J. Maruyama, S. Iwasaki, S. Maruyama, Y.H. Shen, H. Uyama, Nitrogen-doped biomass/polymer composite porous carbons for high ferpormance supercapacitor, J. Power Sources 364 (2017) 374–382.
[8] G. Wang, L. Zhang, J. Zhang, A review of electrode materials for electrochemical supercapacitors, Chem. Soc. Rev. 41 (2012) 797–828.
[9] M.X. Yu, L. Zhang, X.J. He, H.H. Yu, J.F. Han, M.B. Wu, 3D interconnected porous carbons from MOF-5 for supercapacitors, Mater. Lett. 172 (2016) 81–84.
[10] H.Z. Wan, J.J. Jiang, J.W. Yu, K. Xu, L. Miao, L. Zhang, H.C. Chen, Y.J. Ruan, $NiCo_2S_4$ porous nanotubes synthesis viasacrificial templates: high-performance electrode materials of supercapacitors, CrystEngComm 15 (2013) 7649–7651.
[11] Y. Huang, J. Liang, Y. Chen, An overview of the applications of graphene-based materials in supercapacitors, Small 8 (2012) 1805–1834.
[12] L.X. Wang, R.R. Wang, H.Y. Zhao, L. Liu, D.Z. Jia, High rate performance porous carbon prepared from coal for supercapacitors, Mater. Lett. 149 (2015) 85–88.
[13] R. Pietrzak, K. Jurewicz, P. Nowicki, K. Babeł, H. Wachowsk, Nitrogen-enriched bituminous coal-based active carbons as materials for supercapacitors, Fuel 89 (2010) 3457–3467.
[14] M.H. Tan, J.T. Zheng, P. Li, N. Tsubaki, M.B. Wu, Preparation and modification of high performance porous carbons from petroleum coke for use as supercapacitor electrodes, New Carbon Mater. 31 (2016) 343–351.
[15] Y.H. Wang, P. He, X.M. Zhao, W. Lei, F.Q. Dong, Coal tar residues-based nanostructured activated carbon/Fe_3O_4 composite electrode materials for supercapacitors, J. Solid State Electrochem. 18 (2014) 665–672.
[16] E. Frackowiak, Carbon materials for supercapacitor application, Phys. Chem. Chem. Phys. 9 (2007) 1774–1785.
[17] W.D. Geng, F.W. Ma, G. Wu, S.J. Song, J.F. Wan, MgO-templated hierarchical porous carbon sheets derived from coal tar pitch for supercapacitors, Electrochim. Acta 191 (2016) 854–863.
[18] C.G. Zhong, S.L. Gong, L.E. Jin, P. Li, Q. Cao, Preparation of nitrogen-doped pitch-based carbon materials for supercapacitos, Mater. Lett. 156 (2015) 1–6.
[19] W.F. Deng, Y.J. Zhang, L. Yang, Y.M. Tan, M. Ma, Q.J. Xie, Sulfur-doped porous carbon nanosheets as an advanced electrode material for supercapacitor, RSC Adv. 5 (2015) 13046–13051.
[20] C.M. Yang, B.H. Kim, Highly conductive pitch-based carbon nanofiber/MnO_2 composites for high-capacitance supercapacitors, J. Alloys Compd. 749 (2018) 441–447.
[21] H. Yu, W.L.T. Li, L. Zhi, L.Q. Dang, Z.H. Liu, Z.B. Lei, Capacitive performance of porous carbon nanosheets derived from biomass cornstalk, RSC Adv. 7 (2017) 1067–1074.
[22] J.F. Li, S.W. Ma, L.Y. Cheng, Q.S. Wu, Egg yolk-derived three-dimensional porous carbon for stable electrochemical supercapacitors, Mater. Lett. 139 (2015) 429–432.
[23] L. Zhang, F. Zhang, X. Yang, K. Leng, Y. Huang, High-performance supercapacitor electrode materials prepared from various pollens, Small 9 (2013) 1342–1347.
[24] L. Zhou, H. Cao, S.Q. Zhu, L.R. Hou, C.Z. Yuan, Hierarchical micro-/mesoporous N- and O-enriched carbon derived from disposable cashmere: a competitive cost-effective material for high-performance electrochemical capacitors, Green Chem. 17 (2015) 2373–2382.
[25] G.X. Zhang, Y.M. Chen, Y.G. Chen, H.B. Guo, Activated biomass carbon made from bamboo as electrode material for supercapacitors, Mater. Res. Bull. 102 (2018) 391–398.
[26] H.F. Ma, Z.B. Liu, X.D. Wang, C.C. Zhang, Supercapacitive performance of porous carbon materials derived from tree leaves, J. Renewable Sustainable Energy 9 (2017) 044105.
[27] J.Y. Qu, C. Geng, S.Y. Lv, G.H. Shao, S.Y. Ma, M.B. Wu, Nitrogen, oxygen and phosphorus decorated porous carbons derived from shrimp shells for supercapacitors, Electrochim. Acta 176 (2015) 982–988.
[28] W.J. Qian, F.X. Sun, Y.H. Xu, L.H. Qiu, C.H. Liu, S.D. Wang, F. Yan, Human hair-derived carbon flakes for electrochemical supercapacitors, Energy Environ. Sci. 7 (2014) 379–386.
[29] H. Zhuo, Y.J. Hu, X. Tong, L.X. Zhong, X.W. Peng, Runcang Sun, Sustainable hierarchical porous carbon aerogel from cellulose for high-performance supercapacitor and CO_2 capture, Ind. Crop. Prod. (2016) 229–235.
[30] Y.J. Hu, X. Tong, H. Zhuo, L.X. Zhong, X.W. Peng, S. Wang, R.C. Sun, 3D hierarchical porous N-doped carbon aerogel from renewable cellulose: an attractive carbon for high-performance supercapacitor electrodes and CO_2 adsorption, RSC Adv. 6 (2016) 15788.
[31] X. Tong, H. Zhuo, S. Wang, L.X. Zhong, Y.J. Hu, X.W. Peng, W.J. Zhou, R.C. Sun, A new strategy to tailor the structure of sustainable 3D hierarchical porous N-self-doped carbons from renewable biomass for high-performance supercapacitors and CO_2 capture, RSC Adv. 6 (2016) 34261.
[32] Z.H. Chen, H. Zhuo, Y.J. Hu, L.X. Zhong, X.W. Peng, S.S. Jing, Q.Z. Liu, X.T. Zhang, C.F. Liu, R.C. Sun, Self-biotemplate preparation of hierarchical porous carbon with rational mesopore ratio and high oxygen content for an ultrahigh energy-density supercapacitor, ACS Sustain. Chem. Eng. 6 (2018) 7138–7150.
[33] F. Béguin, K. Szostak, G. Lota, E. Frackowiak, A self-supporting electrode for supercapacitors prepared by one-step pyrolysis of carbon nanotube/polyacrylonitrile blends, Adv. Mater. 17 (2005) 2380–2384.
[34] J. Chmiola, G. Yushin, Y. Gogotsi, C. Portet, P. Simon, P.L. Taberna, Anomalous increase in carbon capacitance at pore sizes less than 1 nanometer, Science 313 (2006) 1760–1763.
[35] F. Gao, J.Y. Qu, C. Geng, G.H. Shao, M.B. Wu, Self-templating synthesis of nitrogen-decorated hierarchical porous carbon from shrimp shell for supercapacitors, J. Mater. Chem. A 4 (2016) 7445–7452.
[36] M. Sevilla, A.B. Fuertes, Chemical and structural properties of carbonaceous products obtained by pyrolysis and hydrothermal carbonisation of corn stover in Australian, Chem. Eur. J. 15 (2009) 4195–4203.
[37] Y.R. Liu, One-pot hydrothermal synthesis of nitrogen-doped hierarchically porous carbon monoliths for supercapacitors, J. Porous. Mater. 21 (2014) 1009–1012.
[38] H.M. Luo, Y.F. Yang, Y.X. Sun, X. Zhao, J.Q. Zhang, Preparation of lactose-based attapulgite template carbon materials and their electrochemical performance, J. Solid State Electrochem. 19 (2015) 1171–1180.
[39] Y.N. Gong, D.L. Li, C.Z. Luo, Q. Fu, C.X. Pan, Highly porous graphitic biomass carbon as advanced electrode materials for supercapacitors, Green Chem. 19 (2017) 4132–4140.
[40] T.X. Shang, X.J. Jin, Waste particleboard-derived nitrogen-containing activated carbon through KOH activation for supercapacitors, J. Solid State Electrochem. 20 (2016) 2029–2036.
[41] J.G. Jiang, L.K. Bao, Y.W. Qiang, Y.C. Xiong, J.Y. Chen, Sol-gel process-derived rich nitrogen-doped porous carbon through KOH activation for supercapacitors, Electrochim. Acta 158 (2015) 229–236.
[42] N. Velmurugan, S.S. Han, Y.S. Lee, Antifungal activity of neutralized wood vinegar with water extracts of *Pinus densiflora* and *Quercus serrata* saw dusts, Int. J. Environ. Res. 3 (2009) 167–176.
[43] G.L. Zhou, J.J. Wu, Z.Y. Miao, X.L. Hu, X. Li, X. Shi, Z.D. Cai, Y.K. Shang, Effects of process parameters on pore structure of semi-coke prepared by solid heat carrier with dry distillation, Int. J. Min. Sci. Technol. 23 (2013) 423–427.
[44] Q. Zhang, K. Han, S. Li, M. Li, J. Li, K. Ren, Synthesis of garlic skin-derived 3D hierarchical porous carbon for high-performance supercapacitors, Nanoscale 10 (2018) 2427–2437.
[45] J.Li. Chang, Z.Y. Gao, X.R. Wang, D.P. Wu, F. Xu, X. Wang, Y.M. Guo, K. Jiang, Activated porous carbon prepared from paulownia flower for high performance supercapacitor electrodes, Electrochim. Acta 157 (2015) 290–298.
[46] J.H. Hou, K. Jiang, R. Wei, M. Thir, X.G. Wu, M. Shen, X.Z. Wang, C.B. Cao, Popcorn-derived porous carbon flakes with an ultrahigh specific surface area for superior performance supercapacitors, ACS Appl. Mater. Interfaces 9 (2017) 30626–30634.
[47] Z. Li, Z.W. Xu, H.L. Wang, J. Ding, B. Zahiri, C.M.B. Holt, X.H. Tan, D. Mitlin, Colossal pseudocapacitance in a high functionality high surface area carbon anode doubles the energy of an asymmetric supercapacitor, Energy Environ. Sci. 7 (2014) 1708–1718.
[48] M. Lu, Y.J. Qian, C.C. Yang, X. Huang, H. Li, X.J. Xie, L. Huang, W. Huang, Nitrogen-enriched pseudographitic anode derived from silk cocoon with tunable flexibility for microbial fuel cells, Nano Energy 32 (2016) 382–388.
[49] M.S. Javed, S.G. Dai, M.J. Wang, D.L. Guo, L. Chen, X. Wang, C.G. Hu, Y. Xi, High performance solid state flexible supercapacitor based on molybdenum sulfide hierarchical nanospheres, J. Power Sources 285 (2015) 63–69.
[50] E.R. Piñero, M. Cadek, F. Béguin, Tuning carbon materials for supercapacitors by direct pyrolysis of seaweeds, Adv. Funct. Mater. 19 (2009) 1032–1039.
[51] Z. Li, Z.W. Xu, X.H. Tan, H.L. Wang, C.M.B. Holt, T. Stephenson, B.C. Olsen, D. Mitlin, Mesoporous nitrogen-rich carbons derived from protein for ultra-high capacity battery anodes and supercapacitors, Energy Environ. Sci. 6 (2013) 871–878.